Next Generation UV
Instrument Technologies

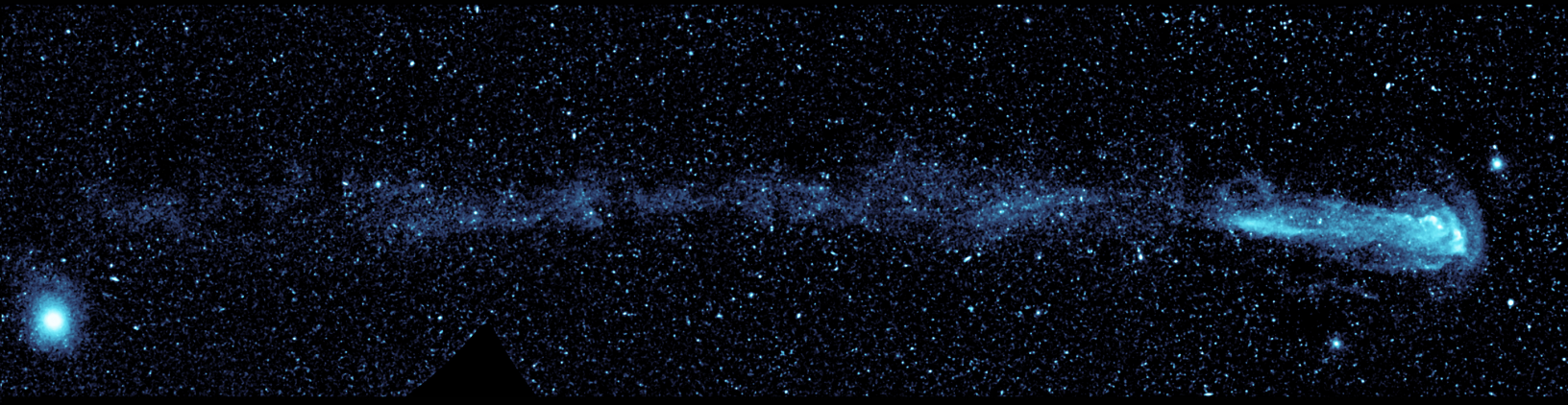### March 2016

Keck
INSTITUTE FOR SPACE STUDIES
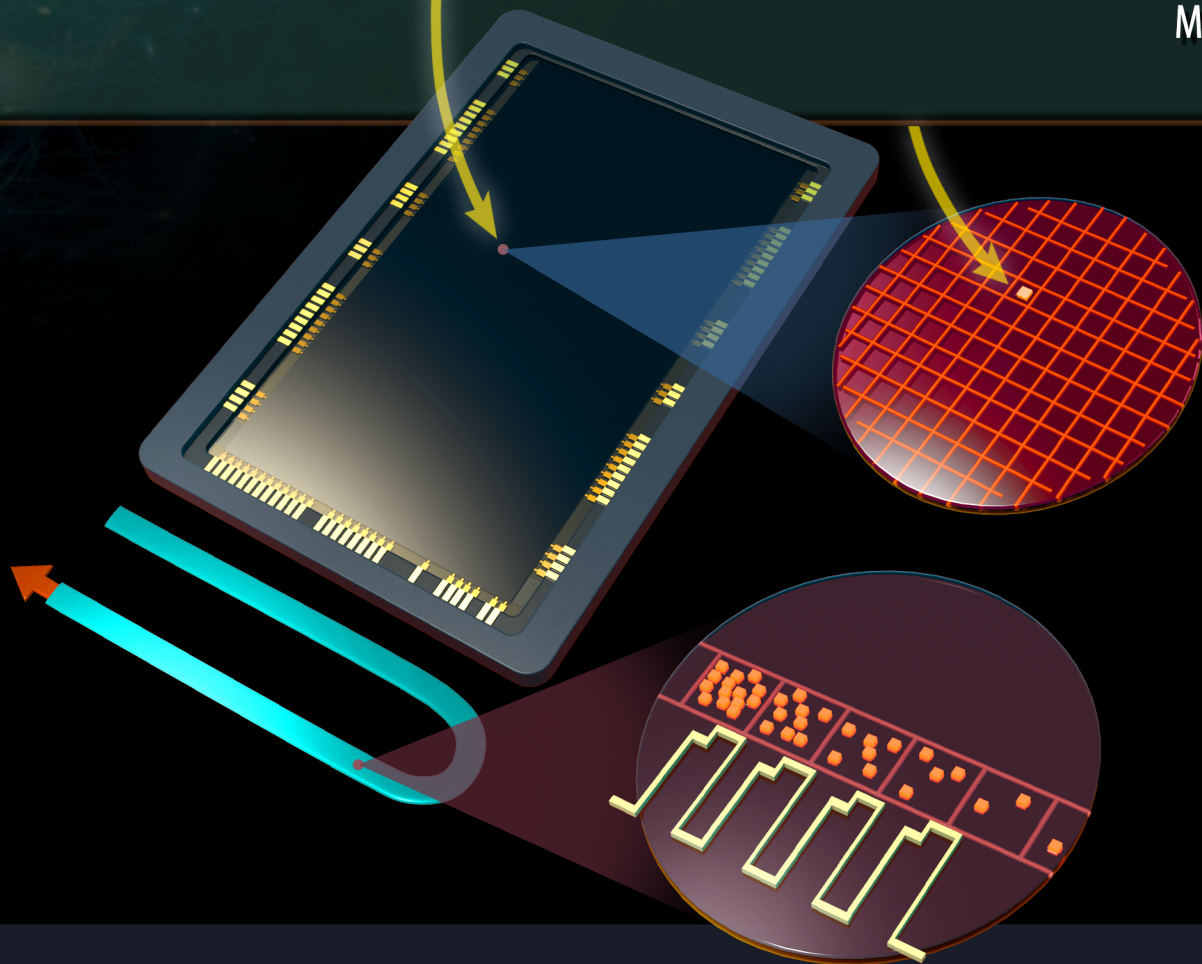
Study Report prepared for the Keck Institute for Space Studies (KISS)

Contents

List of Figures

Technical Development List of Participants

JPL/Campus/External Participants

Caltech PI
Chris Martin

JPL PI
Shouleh Nikzad

Co-Investigators
Patrick Morrissey (Caltech)
David Schiminovich (Columbia University co-PI)

JPL Team
April Jewell, Chaz Shapiro, Sam Chang, Tim Goodsall, Todd Jones, Michael Hoenk

Caltech Team
Matt Matuszewski, Don Neill, Marty Crabill

Columbia Team
Michele Lemon, Hwei Ru Ong, Sam Gordon

Graduate Students & Postdocs

Nicole Linger, Caltech graduate student. Defending in the next 6 months

Jose Zorilla, Columbia graduate student

Erika Hamden, Caltech Postdoc (formally Columbia graduate student, now independently funded by NSF AAPF and Millikan Prize)

Gillian Kyne, Caltech Postdoc

Executive Summary

Goal of program

Our objective is the development of high-efficiency, low-noise photon-counting UV CCD detectors. This is accomplished via delta-doping and anti-reflection coating (ARC) developed at JPL, with testing at JPL and Columbia, combined with low noise electron multiplying charge-coupled device (EMCCD) technology, tested extensively at Caltech. This development work has resulted in detectors with low noise, low dark current, high UV efficiency, and high quality surface cosmetics.

Key Areas of accomplishment

Our technical development program has directly led to advancement in several key areas, described briefly below and expanded in greater detail in Chapter 2.

1. Successful delta-doping of large area array e2v EMCCD CCD201-20 **(JPL)**

2. Successful multi-layer AR coatings, including single, 3-, and 5-layer AR coating development **(JPL and Columbia)**

3. Successful integration of 5-layer AR coating and delta-doped e2v EMCCD; quantum efficiency (QE) tests from e2v **(JPL)**

4. Successful demonstration of end-to-end wafer-level EMCCD processing for far ultraviolet with co-support from SAT **(JPL)**

5. Extensive testing of engineer-grade e2v EMCCD ccd201-20 **(Caltech)**

6. Ongoing testing of noise performance of delta-doped AR coated EMCCDs **(Caltech)**

7. Sky testing at Palomar **(Caltech and JPL)**

Each advancement listed above represents a crucial requirement on the path to achieving flight-qualified high efficiency UV-optimized EMCCDs. The development work at JPL has resulted in robust, reliable devices with good cosmetics, HV clock responses, and excellent UV performance. The testing at Columbia, in collaboration with Caltech, has yielded high-quality ARC and helped to optimize atomic layer deposition (ALD) of coatings. Noise testing at Caltech includes the lowest measurements of dark current yet, with additional improvement of waveform shaping through variable clocks. The end result is a detector which can achieve nearly all the flight requirements for the upcoming balloon flight of the Faint Intergalactic-medium Redshifted Emission Balloon (FIREBall, Sept. 2016), for future Medium explorers (MIDEX, Announcement of Opportunity (AO) in winter 2016), and for medium- and far-term missions likely to be recommended by the 2020 Decadal Survey.
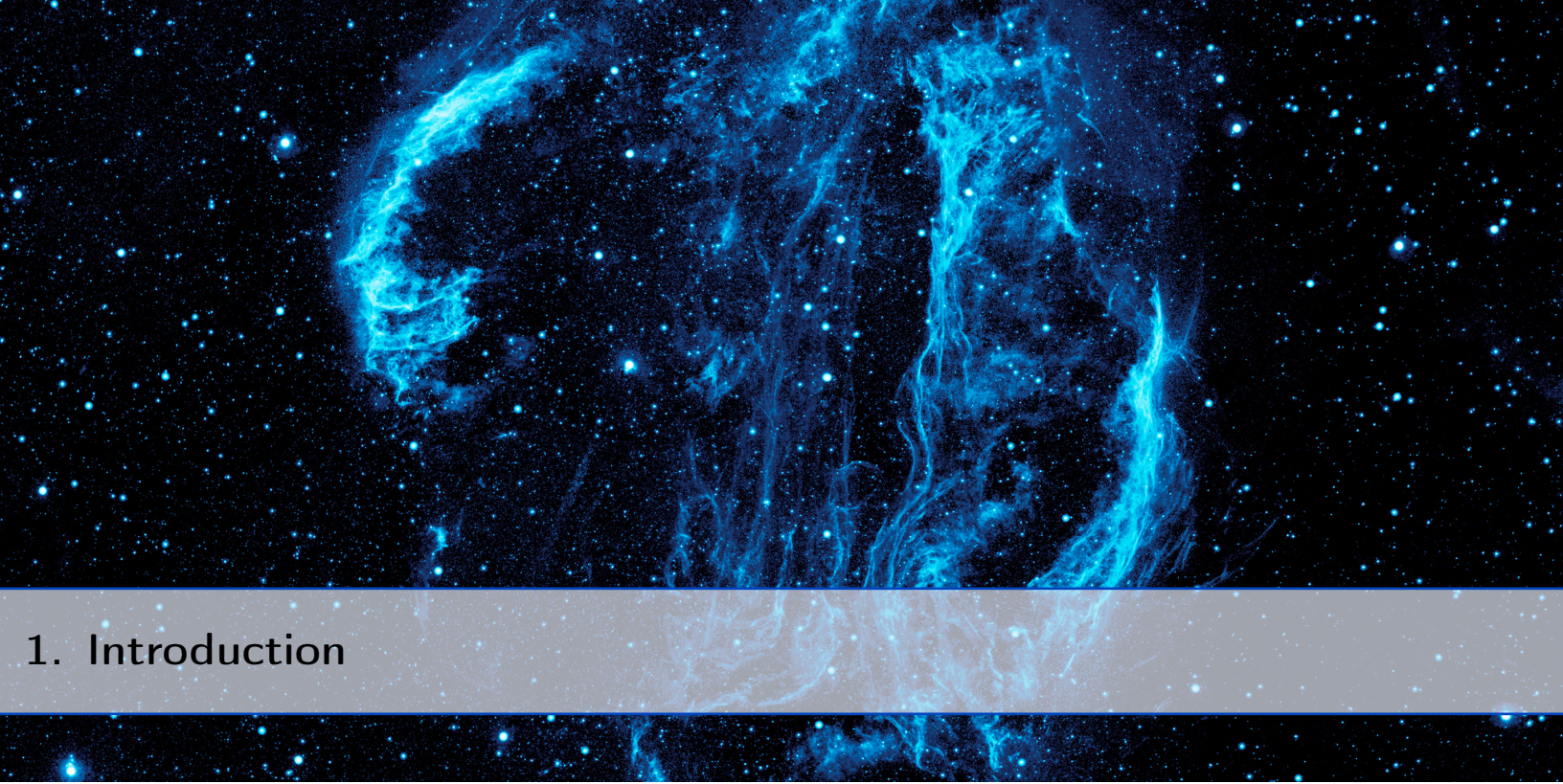
1. Introduction

Our initial KISS Study focused on next-generation UV instrument technologies to enable missions in astrophysics, cosmology, and planetary science. This Study sought to create a new paradigm in UV instrument design, detector technology, and optics. Part of the motivation for the Study was scientific, as the UV range remains relatively unexplored compared to other wavelength ranges and there are significant observational programs that remain to be conducted. Furthermore, likely budget limitations for future missions will require scientists to squeeze every possible photon out of future endeavors. Both of these motivations indicate that there are significant scientific rewards to be gained in UV technology development.

1.1 Initial KISS Study on UV Single Photon Counting Detectors

Our KISS Study identified a portfolio of UV technologies that will enable and revolutionize the next generation of UV astrophysics, planetary, heliophysics, and Earth-observing missions. We developed ideas and identified technologies with the highest scientific impact, that are near a tipping point in their development timeline, and that can be progressed with modest, targeted investments of funding from various sources. Because UV photons are absorbed in the very first few nanometers of most materials, nanotechnology tools and nano-engineered surfaces are fundamental to the most promising technologies. Some of the technologies studied have been demonstrated as a proof of concept, and with modest investments can be brought front and center to play a major role in future mission development. Others are fairly or completely new, either developed only at the concept level or conceived at the KISS workshop itself. From this portfolio of technologies, spanning a broad range of development stages, we have selected the subset that is most likely to lead to near-term breakthroughs if supported by KISS Technology

Development Funding. In combination, these modest investments have an enormous potential payoff. Table 1 summarizes our development plan, as well as potential impacts on instrument and mission performance and affordability.

Technology	Readiness/ Funding	Proposed Development	Institution	Mission Enabling Factor
SPUD: Single Photon counting UV Detector	TRL3/This development fund	Custom EMCCD wafer/device design Flight packaging Delta-doping AR Coating Environmental testing Functional testing (QE, Noise, DR)	Caltech/e2v JPL JPL/MDL JPL/Columbia U. JPL Caltech	5–10[a]
ALD Coatings	TRL1/SAT etc.	Broad-band/High R/Low phase error coating Narrowband and Red-blocking	JPL/CU/Columbia JPL/Columbia	3[b]
EBL Gratings	TRL2	3 test rulings Measure efficiency, scatter	JPL U of Colorado (CU)	2–4[c]
Nanodetectors: UV/Visible discrimination	TRL0	Perform theoretical modeling/Fabricate test device	JPL: Seek fund from JPL spontaneous RTD or CIF	?
Total		Data grasp ($A_{\mathrm{eff}} \times N_{\mathrm{objects}}$) factor	20–250	
Improvement		Aperture reduction factor (linear): F_A	2–4	
Factor		Cost reduction factor: F_A^2	4–16 (e.g., 10B\$ →600M\$–2.5B\$)	

Table 1.1: Mission & Discovery Enabling UV Technology Development Plan

[a]Improvement from quantum efficiency enhancement over existing UV photon-counting detectors. Improvements in signal-to-noise ratio may exceed this factor because of lower dark noise.

[b]Improvement in total reflectivity of a 3-reflection telescope and a 5 reflection wide-field, multi-object, high-resolution, aberration-corrected UV spectrograph.

[c]Improvement in groove efficiency and total reflectivity for high-dispersion diffraction gratings (×2) and improvement in field-of-view of aberration-corrected wide-field UV spectrograph using arbitrarily curved grooves.

Our highest priority objective is the development of high-performance UV-optimized EMCCDs. These devices will enable breakthrough UV capabilities in future UV spectroscopic and imaging missions. One of the principal objectives of these missions will be UV spectroscopy of the intergalactic medium (IGM) in absorption and emission. A factor of 10–20× improvement in detector efficiency corresponds to a 3–4.5-fold reduction in telescope size for the same mission performance. Using a conservative scaling, a 4–6-m aperture combined with Gen-1 UV detectors would cost \$2.5-5B, while a 1.4-m UV spectroscopy mission using the NEXUS detector and equivalent total efficiency would cost only ~\$500M and qualify as a probe mission!

1.2 Frontier Science Measurements Enabled by KISS UV Development

We stand on the threshold of constructing a complete picture of the origin and evolution of the Universe. The conditions that seeded the growth and evolution of large-scale structure, galaxies, and their constituents are known from studies of the cosmic microwave background. Major efforts are underway to understand the nature of the dark energy that dominates the mass-energy density of the Universe, and the nature of the dark matter that drives structure formation. The Hubble Space Telescope (HST) and the Keck Observatory have delineated the history of galaxy formation and evolution, and future planned observatories such as the James Webb Space Telescope (JWST) and the Thirty Meter Telescope (TMT) will search for the first star clusters and galaxies to complete this history.

The next step, and the grand challenge of the next few decades, will be to explain this cosmic history. How does matter, starting from an astoundingly tenuous state, collapse by 24 orders of magnitude in density to ultimately form stars and planets? How does the nebulous IGM collapse into a cosmic web of filaments, in which gas flows to form and fuel galaxies over cosmic time? How does gas flow in and out of the circumgalactic halos of galaxies, with inflows fueling star formation and outflows from galactic superwinds seeding the IGM with new chemical elements? How does gas flow within galaxies and collapse in star forming complexes, thus regulating the ongoing growth of galaxies? How do protostellar clouds collapse to form both massive and low mass stars, and how do protostellar disks grow and ultimately form planetary systems?

These questions of cosmogony engage a large, multi-wavelength segment of the astrophysics enterprise. Of special relevance, there are particularly compelling, broad, and definitive measurements that can be made with new space missions in the optical/near-IR and especially the ultraviolet (UV) wavelength ranges. Discoveries from UV-capable astrophysics missions in the last decades—notably the Far Ultraviolet Spectroscopic Explorer (FUSE, Moos et al. 27), HST, and the Galaxy Evolution Explorer (GALEX, Martin et al. 22, Morrissey et al. 28)—as well as from rest-UV observations of the high redshift universe in the optical, have demonstrated that UV observations have enormous diagnostic power to trace gas and star formation over an enormous range of scales and densities. Theorists now predict that UV emission will yield a completely new and informative picture of the growth of structure in the Universe from the IGM to planets.

To date, all UV measurements have been based on technologies developed in the '60s and '70s, and are thus profoundly limited in sensitivity and scope. UV technology has been limited by low quantum efficiency, low reflectivity, high background, modest fields of view, and spectral multiplexing—all areas in which we are poised to make gigantic strides. Modest investments in new UV technology will enable groundbreaking new UV missions that can begin to answer the age-old questions of cosmogony in the next 10–20 years, questions that cannot be fully addressed with any other observation. The goal is to enable revolutionary, not incremental, new measurements that unite the entire community and justify the high cost of new missions.
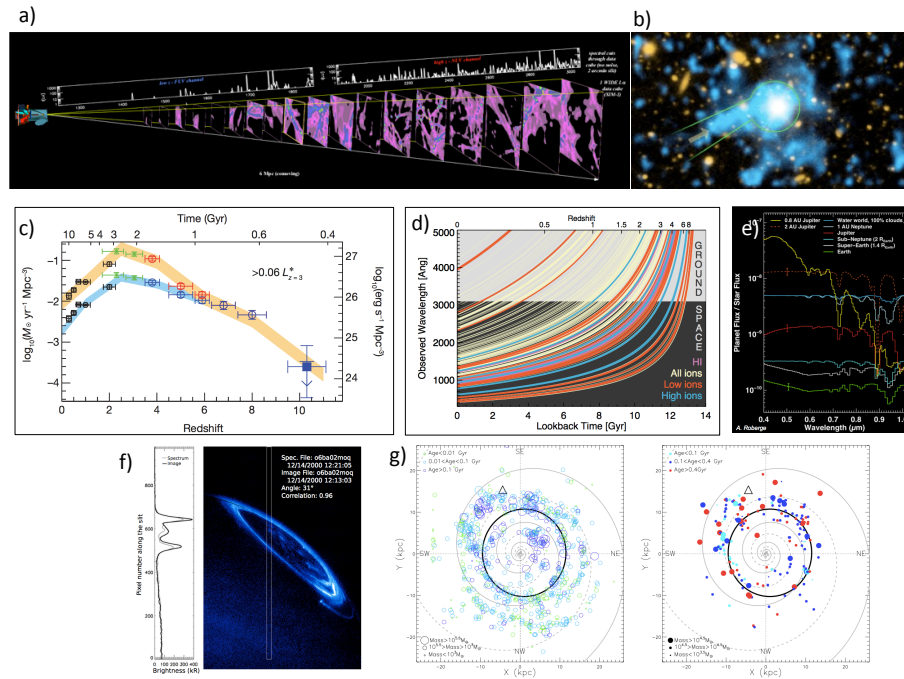
Figure 1.1: a) Artists conception of a UV Explorer with IFU for detection of emission from the IGM/CGM around low z galaxies. C. Martin. b) Martin et al. [23], 2014–QSO HS1549+19 with evidence for inflowing gas/gas disk around z~2.8 quasar. Similar CGM and IGM emission is likely also present at lower redshifts at UV wavelengths. c) Star formation history through cosmic time. UV measurements of star formation for low z galaxies are critical to understanding the star formation history of the universe. Bouwens et al. [4] d) Accessibility of emission lines vs. wavelength and redshift. The space UV provides an important window at nearly all redshifts. Dalcanton et al. [9] e) Simulated R=70 planet spectra for a 2.4m mission. A. Roberge f) UV emission from Jupiter's aurora. Bonfond et al. [2] g) De-projected spatial distribution of UV star forming regions and young clusters from M31. Kang et al. [20]

We note that UV measurements, because of their exquisite sensitivity to atomic, ionic, and molecular constituents over a wide range of temperatures, will continue to be a key component of planetary and heliophysics missions in the future, and therefore will greatly benefit from technology developments driven by the photon-starved astrophysics applications.

Exploring and explaining the life cycle of baryons, from the most diffuse parts of the intergalactic medium to high-density planets and stars, is a central overarching theme of the NASA Astrophysics Program. Of import to both NASA and the world at large, finding earth-like planets and imaging their atmospheres is a key driver of both technology development and instrument design. Figure 1.1 shows just a fraction of the scientific drivers in the UV. Additional drivers are discussed below.

Component				
Property	**Cosmic Web**	**Web/ Halos**	**Dark Halos**	**Galaxies**
Baryon & structure tracer	IGM *fuel*	WHIM *baryons metals*	CGM *infall winds metals*	XUV disk *gal. winds, SF*
δ	1-100	1-100	10^2-10^5	$>10^6$
Size [Mpc]	0.3-30	1-30	0.1-0.3	0.03-0.1
T[K]	10^4-10^5	10^5-10^7	10^4-10^6	
QSO absorption	Lα forest	OVI, broad Lα	Ly limit Metal lines	Damped Lα
Emission	Photon pumping (PP)	Collisional excitation (CE), PP	CE, PP,Lα fluorescence	UV cont CE from feed-back
Intensity [LU]	1-100	1-100	10^2-10^4	

Figure 1.2: Components of the CGM and IGM, with estimated intensities, sizes, and emission mechanisms.

1.2.1   Mapping the Flow of Baryons through Cosmic Time

Large-scale models of the Lambda cold dark matter (ΛCDM) universe predict a familiar structure: sheets and filaments of dark matter arranged in a "cosmic web," galaxies and clusters residing along the web and at its nodes. Channeled along the web by gravity, baryons flow into galaxies and are later transformed and ejected by stellar winds, supernovae, and galactic activity. These "feedback" processes inject energy and metals into the galaxy halo and nearby IGM, but are very poorly understood considering their importance to numerical simulations, which use feedback prescriptions to predict fundamental properties such as the size, angular momentum, and luminosity function of galaxies [18, 11].

A summary of the physical components of the IGM, their relationship to galaxies, and observational signatures is shown in Figure 1.2. The structure we describe has been inferred from indirect measurements such as quasar (quasi-stellar obects, or QSO) absorption line spectra. Recent work mapping emission directly has provided further hints of the complex IGM environment [5, 23, 24].

Most of the IGM consists of moderately over-dense gas ($1 < \delta < 100$) ionized by the metagalactic UV background (UVB) and continuing to expand with the Hubble flow. Trace neutral hydrogen in the cosmic web is responsible for the Lyman-α "forest" observed in QSO absorption line spectra.

The forest provides a powerful constraint on large-scale structure and cosmology, since simulations show that IGM baryons trace dark matter. There are metals in the cosmic web, suggesting early and ongoing enrichment by galactic winds. At $z = 0$ we suspect most baryons have collapsed into a Warm-Hot Intergalactic Medium (WHIM, $T_{vir} \sim 10^5$–10^7 K,) which produces weak, broad, difficult to detect Ly-αabsorption, and most of the $z \sim 0$ OVI absorption [35, 37, 17, 31].

Galaxies and groups form in dark matter halos ($\delta > 100$) in the denser parts of web filaments and nodes. The uncollapsed circumgalactic medium (CGM) gas within halos may be in-falling from IGM filaments, cooling and collapsing onto the galaxy to fuel star formation, stripped from merging subsystems, or ejected and heated by galactic winds. Denser CGM gas may be detected as Lyman limit systems ($N_{HI} > 10^{18}$ cm^{-2}), metal line absorbers (MgII, CIV, some OVI), and Damped Ly-αsystems (DLA; $N_{HI} > 10^{20}$ cm^{-2}).

1.2.2   Understanding Cycles of Star Formation, Enrichment, & Feedback into/out of Galaxies

In our quest to understand the forces that drive galaxy evolution and the conversion of baryons into stars, we turn to galaxies themselves, and in particular to the forces driving star formation. These can be studied in a powerful new way with new UV and advanced optical-infrared (OIR) capabilities. HST has proven the importance of OIR imaging for mapping the growth of galaxies over cosmic time. GALEX has shown the power of UV imaging to delineate star formation across an enormous range of physical regimes, from the lowest to the highest mass, from extremely low levels of star formation tracing the final trickle of gas from the IGM to the massive starbursts that dominated galaxy growth in the "epoch of star formation." High resolution, wide-field UV imaging will probe star formation in all of its variations and modalities on scales small enough to delineate the physical triggers, and—in samples numerous enough to separate the influence of environment—local gas density, local stellar and gas velocity dispersion, gravitational instabilities, and local gas flows in determining the local and global star formation history in galaxies. Resolved UV stellar photometry could be exploited in future missions to deconstruct the recent star formation history and initial mass function in diverse physical regimes of a representative set of nearby galaxies.

UV spectroscopy of galaxies has lagged behind other techniques because of the limitations of UV technology. This situation is unfortunate since UV spectra harbor a cornucopia of physical diagnostics. UV spectra probe the age, metallicity, and stellar mass distribution in newly formed stars, the distribution, dynamics, and chemical abundances of the ISM from which these stars form, and the local and global impacts of stellar feedback in regulating star formation and driving gas flows in and out of galaxies. UV spectroscopy measures the all-important Lyman-alpha line of hydrogen. Mapping the spatial and kinematic distribution of this line in lower redshift galaxies may be the only way to interpret this strong line in the most distant, youngest galaxies observed by Keck, JWST, and TMT. Galaxies may have been responsible for reionizing the Universe at
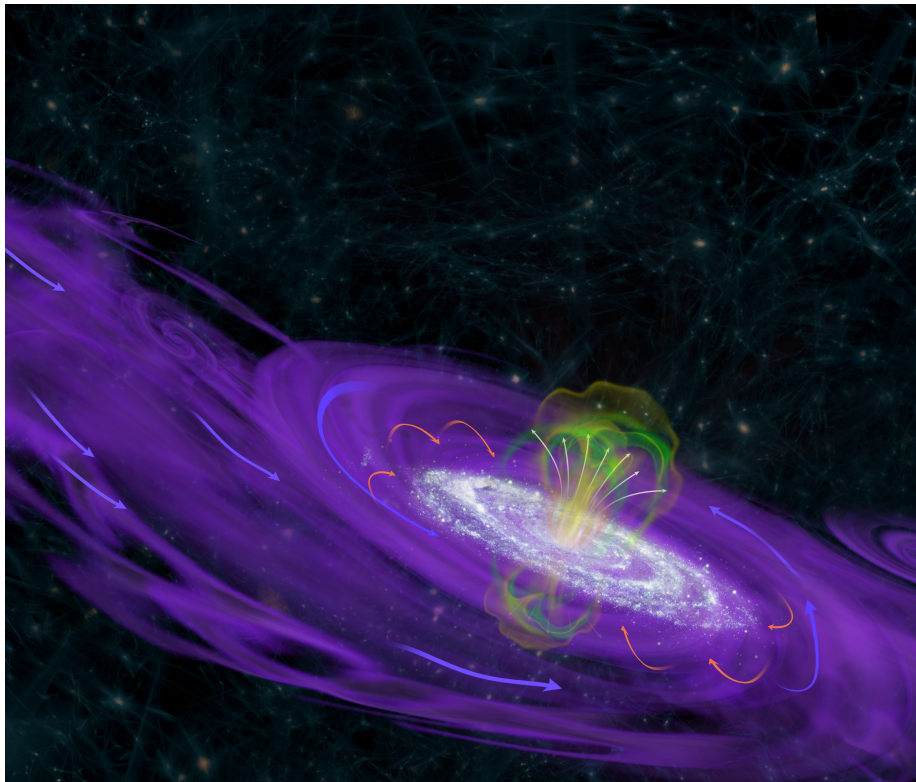
Figure 1.3: Artist's interpretation of the complex gas flow around a spiral galaxy. Inflowing and outflowing gas can be seen in purple and green, respectively. The inflowing gas is spiraling around and into the galaxy, feeding star formation within the galaxy and creating complex structures recently mapped by Martin et al. [24]

redshift z 8, which can only be the case if ionizing radiation from young, massive stars can escape the ISM of the galaxies. Understanding this escape may only be possible in nearby galaxies that can be spectroscopically mapped in Lyman continuum (escaped ionizing) radiation.

Wide field UV imaging requires large-format, low-noise detectors with high quantum efficiency (QE) and good red rejection from the detector or efficient UV filters. High-resolution imaging is far more sensitive with photon-counting detectors because of the very low UV sky background. Wide-field, imaging, and highly-multiplexed UV spectroscopy requires the highest QE, low background, photon-counting detectors that can be assembled in large formats with high pixel counts in order to span broad wavebands simultaneously with large fields of view and spectrum count. These high-performance wide-field spectrographs in turn require highly efficient UV coatings that support multi-optic, highly corrected designs.

1.2.3   Discerning the Formation & Evolution of Stellar, Protoplanetary, & Planetary Systems

We seek to understand how matter collapses from giant molecular star-forming clouds to form protostars, protostellar and protoplanetary disks, stars, and ultimately planets. While some of these phases are shrouded in UV/optical absorbing dust and can only be studied in the Far IR and radio bands, key evolutionary stages become visible in the UVO as the enshrouding dust is disrupted by feedback from the protostars. GALEX has shown that UV imaging allows us to quickly identify chromospherically active stars that are young and likely to harbor planets in the early stages of evolution, perhaps still radiating gravitational collapse energy. High resolution and high contrast UVO imaging and spatially resolved spectroscopy allows us to image and spectrally map protostellar jets, in order to understand the regulation of stellar mass by feedback. High resolution and high contrast UVO imaging and spatially resolved spectroscopy of protostellar/protoplanetary disks (PPDs) will allow us to directly search for structures indicating planet growth.

The lifetime, spatial distribution, and composition of gas and dust in the inner ~10 au of young (age $<$ 10 Myr) circumstellar disks are important components of our understanding of the formation and evolution of extrasolar planetary systems. Molecular and atomic lines in the far UV (H_2, CO, CIV, etc.; 100–170 nm) trace disk gas and accretion timescales. For mature exoplanetary systems, transit spectroscopy enables a direct measurement of atmospheric composition and mass loss from extrasolar giant planets. The FUV band (115–170 nm) provides access to resonance line diagnostics of the primary atmospheric species (hydrogen, carbon, oxygen, etc.) that are not readily observable at other wavelengths.

1.2.4   Detection & Characterization of Exoplanets

A primary goal of the next large optical observatory is direct imaging and spectroscopic characterization of nearby Earth-like planets. This will require a large ($\gtrsim$ 4-meter) aperture and some combination of ultra-high-contrast internal coronography and/or an external occulter. The UVOIR and Exoplanet communities recognize that a large UVO mission almost certainly can only take place as a combined general-purpose UVO observatory and a terrestrial planet imaging and characterization mission.

Ultraviolet spectra are critical to our understanding of Earth-like worlds, particularly in light of the growing number of Earth-like planets detected orbiting low-mass stars [3]. A major source of uncertainty regarding the habitability of these worlds is the strength and variability of the local radiation field where liquid water can persist (the "habitable zone"). Ultraviolet radiation is important to the photodissociation and photochemistry of H_2O and CO_2. It also enables the synthesis of biomarkers, including CH_4 and O_3. Stellar flares may imbue the exoplanetary atmosphere with heavy doses of ultraviolet radiation, potentially catalyzing or retarding the development of biology on these worlds.

1.2.5 Solar System UV Science

Our solar system, and the bodies and processes within it, form the critical link between our understanding of Earth and its evolution and exoplanets, stellar formation, and the IGM. Ultraviolet spectroscopy is an essential method for probing solar system targets. Hubble Space Telescope discoveries have been crucial in furthering our knowledge of dynamic processes in a number of scientific areas within the solar system, and have been key in driving follow-on planetary missions. The importance of a space-based UV facility for planetary studies was called out in the Planetary Decadal Survey (Visions and Voyages for Planetary Science in the Decade 2013-2022[1]). Key planetary scientific areas include auroral studies at bodies such as Jupiter, Saturn, Io, Europa, and Ganymede [2]; atmospheric studies at Venus, Titan, the gas giants (Jupiter, Saturn), and ice giants (Neptune, Uranus), as well as thinner atmospheres (Mercury, Mars, Ganymede, Io, Pluto); cryovolcanism studies and searches (Europa, Enceladus, primitive bodies, and other moons); neutral and plasma torus investigations; and studies of comets. For example, the dynamics of auroral and airglow spectral (100–350 nm) and brightness distributions reveals magnetospheric interactions with the solar wind and with planetary satellites. Ultraviolet stellar occultations discovered the spatially-confined cryovolcanic plumes in the south polar region of Enceladus and can be further utilized to search for and study activity at other small bodies. Furthermore, the density, thermal, and compositional profiles of planetary atmospheres (including tenuous atmospheres) are probed with high vertical resolution using UV stellar occultations. Investigations of the surface compositions of the wide range of small primitive bodies throughout the solar system (NEOs to main-belt asteroids, Trojan asteroids, and KBOs) can be studied using the previously unexploited UV-visible region, as many of these bodies are still not understood and are often not spectrally active except in the UV-visible. Thus, understanding this spectral region and its implications for surface composition, including organics and volatiles species, is important for understanding the history of our solar system.

1.2.6 Opening Discovery Space

Remarkable new discoveries by GALEX and HST/COS have reminded us that large increases in observational capability lead to new discoveries. The UV technologies we have identified will facilitate large advancements in sensitivity and field of view, and enable highly multiplexed spectroscopy. Wide-field, high angular resolution, time-resolved UV imaging and spectroscopy on multiple timescales will allow the discovery of new UV variable and transient phenomena. There are multiple science drivers for such a survey, including the discovery of new phenomena associated with active galactic nuclei (AGN), supernovae, gamma-ray bursts, accretion disks, flare stars, stellar atmospheres, compact objects, and more.

---

[1]`http://solarsystem.nasa.gov/docs/Vision_and_Voyages-FINAL.pdf`

Variability is one of the hallmark properties of AGN; in fact, it was because of their extreme, often short-timescale variability that AGN phenomena were first associated with black holes, due to the extreme compactness of the emission regions. A UV variability survey would probe several of the regions necessary for understanding AGN.

Two exciting areas of transient research follow GALEX discoveries. Tidal capture flares result when a massive but invisible black hole (AGN) tidally disrupts a star and accretes its gas, forming a several-month-long event that peaks in the UV. The properties of the event determine the black hole and stellar mass, and the rates provide a measurement of the demographics of otherwise silent massive black holes. Supernova explosions begin with a "shock-breakout" event: the core-collapse implosion creates a reverse, outwardly-propagating shock wave through the stellar envelope, dramatically heating the photosphere to UV-emitting temperatures. An initial very bright but very short (minute-long) "spike" has yet to be observed, and will provide strong constraints on the supernova and its progenitor star.

1.3   Single Photon Counting UV detector advantages

The scientific motivations described in Section 1.2 all require a high QE UV detector with low noise and background rates capable of photon-counting. Ideally these detectors would also be large format to support wide field imaging and multi-object spectroscopy. There are a number of heritage UV detectors which were thoroughly explored in the report from our KISS Study. These can be classified into two major categories: 1) vacuum tube technology, which uses a UV sensitive photo-cathode with a gain component coupled to an electron detector, and 2) solid-state devices based on silicon or other wide band-gap semiconductors. Traditionally, the low QE of photo-cathode-based detectors has been far outweighed by their photon counting abilities.

1.3.1   Alternative UV Detectors

Used on most major UV space telescopes in the last 25 years, microchannel plates (MCPs) have been the go-to detector for UV instrument designers for many years [28, 13, 12]. Flight heritage, low red response, and non-zero UV response are all important reasons they continue to be used, but the primary advantage has been the ability to count photons with low noise. MCPs have well known limitations, including requiring high voltage, technically challenging production, gain sag, and a maximum count rate that limits observations of bright targets. The MCP flown on the Juno mission has an average QE of 25% [12]. Recent MCP results have reached as high as 40% QE at 1,000 Å in lab tests with a secondary electron emissive ALD layer and a CsI photocathode [32]. CCDs have not been able to compete in the UV range primarily due to low efficiency and noise limits. Thanks to a concerted development effort yielding better quantum efficiencies and

noise performance, delta-doped UV-optimized EMCCDs are now in a position to challenge MCP dominance in the world of UV photon counting.

A rival technology in photon-counting detector space is the superconducting Microwave Kinetic Inductor (MKID, [10, 25]). MKIDs work using a superconducting inductor whose surface impedance changes upon absorption of a photon. This change can be measured and a rough energy level of the photon can be determined (with R $\sim$ 15 as the current best). MKIDs have the potential to be extremely powerful from the x-ray to the mid-IR, providing a low resolution spectrum without additional optics or grating. The development of MKIDs is still in the very early stages, however. Their small detection area relative to pixel size means each pixel requires a microlens to increase the overall fill factor. The microlens limits the wavelength range at which an MKID could be used, notably cutting off before UV wavelengths. Additionally, large scale imagers still need to be tested and the current pixel failure rate of around 20% needs improvement. Finally, operational challenges such as the necessity of keeping the detector at superconducting temperatures means we are still a long way off from using these detectors in a space environment. Nevertheless, in the long term, MKIDs will be an important component in the instrument designer's toolbox. In the short term, they are not able to replace MCPs or even the current UV-optimized EMCCDs.

1.3.2 Advantages of EMCCDs for Future Instruments & Missions

EMCCDs amplify the signal from a single photoelectron to a value much larger than the on-chip amplifier read noise. This process means single events can be detected by a threshold process described more thoroughly in recent works [34, 16]. Briefly, pixels with counts greater than 5 times the read noise are considered to have detected one photon. Pixels with counts less than this threshold are considered to have zero detections.

The amplification process can be adjusted by changing the voltage of the High Voltage clock in the waveform script, providing an easy way to quickly modify the amount of amplification to reflect the application. At the extreme end of this adjustment, very bright targets can be observed without any amplification, turning the EMCCD operationally back into a normal CCD. Thius, an EMCCD has an extremely wide dynamic range, able to make observations in low light levels with amplification and able to be used in normal mode. This flexibility can be extremely useful on a mission which may need to switch between both modes to fulfill science requirements.

Finally, the operation and manufacturing of an EMCCD is only slightly different than that of a normal CCD. Large scale, wafer-level processing is possible, which lowers overall device costs and encourages using multiple devices in focal plane arrays.

Some drawbacks are inevitable in any technology and EMCCDs have a number of additional complications created by the amplification process. First, not all electrons in the device will be
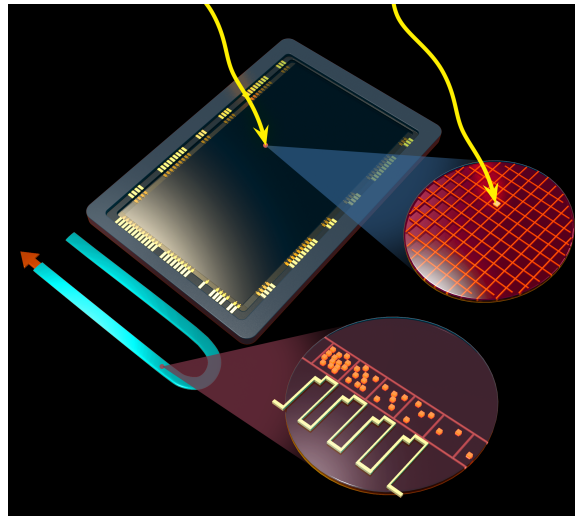
Figure 1.4: Artist's rendering of a delta-doped EMCCD, with photon and associated photo-electron. Insets show the photoelectron in a pixel in the image area and the serial register with gain amplification multiplying photons.

amplified above the 5 sigma threshold. The multiplication process is stochastic, so some fraction of real photoelectrons will not be multiplied enough to be detectable above the read noise. The ratio of the EM gain to the read noise provides an estimate of the number of events that are not counted due to low amplification, as described by [7]. Additionally, added noise comes from clock induced charge (CIC) and dark current. In a standard CCD, when cooled below -85°C and with normal trapezoidal or square clocks, the noise from dark current will only be a few electrons per hour and CIC will be lower than the added read noise (assuming a few electrons of read noise), and thus undetectable. For an EMCCD, both of these noise sources will be amplified in the same manner as photoelectrons.

Dark current can be reduced by operating in inverted mode and by cooling the device further. Recent work exploring the dependence of dark current on temperature indicate a lower limit [33, 6]; however, most applications operate at -85°C and the behavior below this temperature has not been extensively investigated.

CIC can be reduced by wave shaping and modification of the well depths. Daigle et al. [8] has reported great success in minimizing CIC through the use of sinusoidal and triangular shaped clocks. Both shapes reduced CIC by nearly a factor of 10 at the lowest readout frequencies. Shaped clocks also did not exhibit increased CIC with decreased pixel readout speed. The HUVD lab will use a controller with variable clock speed (between 1 and 10 MHz) and wave shaping capabilities to explore ways to minimize CIC while not sacrificing charge transfer efficiency (CTE) or dark current.

EMCCD technology has the ability to transform observations in several regimes:

1. Low surface brightness objects such as the diffuse CGM and IGM, as well as direct detection of planets via direct imaging, where current observations hit hard noise limits.

2. High cadence astronomy where exposure times are extremely short, limiting the number of photons that can be detected.

3. Ultra-high resolution spectroscopy where bright targets are sufficiently spread out that no pixels see rates above the confusion limit.

Many more applications may exist for EMCCDs, but the full parameter space of where these devices can best be utilized will only be fully realized as they are brought into greater use.

1.3.3   EMCCDs: Opening a New, Low Noise Regime for CCDs

Electron multiplied CCDs (EMCCDs), developed in two different designs by e2v and TI, leverage all the advantages of the mature CCD technology while enabling single photon detection by adding a gain register after the serial register of the CCD (at the end of the charge transfer) prior to the readout amplifier. At each stage of this gain serial shift register, a higher gate voltage in the second serial clock phase (~40 V) causes an avalanche effect, producing a small gain in each charge transfer and resulting in a final gain of more than one thousand. Single electron signals are amplified far above the read noise floor and read out through a discriminator, effectively eliminating read noise. EMCCDs can operate with a range of gain from 1,000 (photon-counting) to 1 (conventional CCD) and can therefore accommodate a wide dynamic range of signal. Faint spectroscopic observations can be observed in full photon counting mode at high gain through a discriminator, and—due to the low counts per pixel—suffers no root-2 multiplication noise penalty. Bright targets are observable in conventional (no amplification) mode. A small subset of intermediate brightness targets can be observed at moderate gain with root-2 multiplication noise.

1.3.4   Delta-Doping to Create a Stable, Highly Efficient Detector

Delta-doping technology, developed at JPL and using molecular beam epitaxy (MBE), uniquely achieves atomic-scale control over the surface band structure of a silicon imaging array, resulting in near-100% internal quantum efficiency from the extreme UV (EUV) through near-infrared regions of the spectrum, very low surface-generated dark current, and elimination of quantum efficiency hysteresis. Delta-doping is versatile and compatible with fabrication at foundries, and it can be applied to practically any fully-fabricated silicon array, as has been demonstrated by its application to various CCD designs and formats, CMOS arrays, and PIN diode arrays.

1.3.5 Atomic Layer Deposition of Anti-Reflection Coatings: New to the UV

Extending high silicon detector QE performance into the UV (especially in the 100–300 nm range) requires expanding the AR coating materials set and coating precision. The index of refraction of silicon is a strong function of wavelength, especially in the UV, and certain materials (in particular hafnium oxide) that are ideal AR coatings from 240–300 nm start to strongly absorb at shorter wavelengths. In this shorter-wavelength range, very thin films of materials such as magnesium fluoride and aluminum oxide behave extremely well. Atomically precise and reproducible AR coatings are required at these wavelengths because changes in thickness of 2 nm or less can cause significant shifts in the peak AR response. ALD is a precision technique, perfectly suited to the material challenges posed in the construction of UV instrumentation. ALD is a thin film deposition technique similar to Chemical Vapor Deposition where a desired film is grown using sequential surface reactions, one monolayer at a time. The properties inherent in the ALD method enable growth of smooth, dense, pinhole free films with angstrom level thickness control over arbitrarily large surface areas. ALD is also well-suited for the growth of multilayer stacks of films with sharp interfaces. This technique is extremely flexible, with nearly every element in the periodic table accessible as an ALD material. While ALD enables careful control of interfaces, it is also sufficiently gentle to allow multilayer ALD films of a variety of materials to be directly grown onto a detector (such as a silicon CCD) to fabricate a simple, compact detector that has the highest possible sensitivity.

2. Outcomes of the Technical Development Program

The technical development program has been an incredible success. JPL's development of the delta-doping process for e2v CCD201-20s required only 3 of the 6 wafers purchased for this work. The main adaptation of the normal process flow has been to tailor the wafer thinning for this device type. Additional tests of ALD growth rates on both Si and SiO_2 substrates were explored more thoroughly, resulting in highly repeatable, conformal coatings which behave as predicted by models. Noise testing at Caltech is the result of several years of development, with a low-noise printed circuit board, NUVU controller, high vacuum dewar, and custom software for analysis. Figure 2.1 shows detectors in various stages of processing and the test set-up at Caltech.

2.1 JPL Delta-Doping & ARC Development for High UV Performance

We have processed 2-megapixel arrays with good functionality, imaging, and QE. We modeled and demonstrated FIREBall AR coatings with several designs on live devices. Our characterization showed peak QE > 75% at ~205 nm. In the original measurements made during prior years of this effort, our characterization showed lower QE than predicted by modeling. We systematically investigated and solved this problem through calibration of our characterization system, maintenance of the molecular beam epitaxy (MBE), rigorous surface preparation investigation, materials and device performance analysis, and a systematic investigation of the ALD processes. These factors were examined with respect to their effect on device performance, and problems were resolved through changes to surface preparation procedures and ALD parameters. Device performance has been independently verified with testing at e2v, Inc.
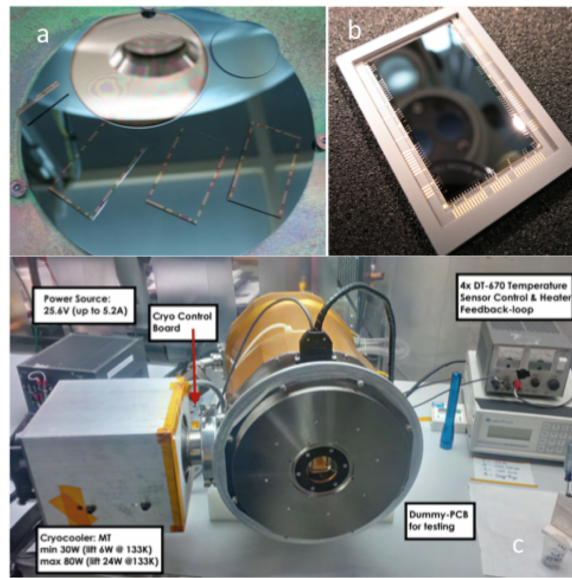
Figure 2.1: a) Three e2v CCD201 die following AT-coating by ALD; the bond pads are exposed prior to the deposition. Several test samples are including for verification. b) fully processed and packaged CCD201-20. c) Test dewar set-up at Caltech with Cryotel cooler.

Under the first year of funding, CCD201-20 wafers were planarized, bonded, and thinned; one was delta-doped at the wafer level. Due to lower than expected device performance, as described above, several die were selected for reprocessing and troubleshooting. Eleven total die were polished to remove the MBE layer in two separate batches (Figure 1); the die were then delta-doped individually. Surface preparation prior to MBE and the MBE growth process itself were reexamined, and new procedures were implemented. Several die were AR coated prior to packaging. Delta-doped devices with narrowband AR coatings (including one-, three-, and five-layer designs) were packaged and tested. "R"-grade 2-megapixel EMCCDs were used as starting devices (the grade is based on vendor probe and number of starting blemishes and defects, not based on the JPL process). Following success with the "R"-grade devices, "G"-grade and "S"-grade devices were delta-doped and AR coated. QE performance at the target wavelength is > 75% (Figures 2 and 3).

In the course of the rest of this development three additional wafers were processed, including one mechanical sample for packaging tests at e2v. It should be noted that the work on the final wafer (and beyond) is continuing under recent funding obtained from NASA's Strategic Astrophysics Technology (SAT). In the subsequent two processing runs, wafers were planarized, bonded, thinned, and delta-doped. Individual die from these wafers were used to develop and optimize the ALD AR coatings. Good functionality and imaging were obtained from a number of devices in these wafers. Based on these results, it was determined that for EMCCDs the thickness of the silicon in the imaging area is a crucial parameter to achieve optimum performance when operated in high-gain mode. This is in part might be due to the use of high voltage in the
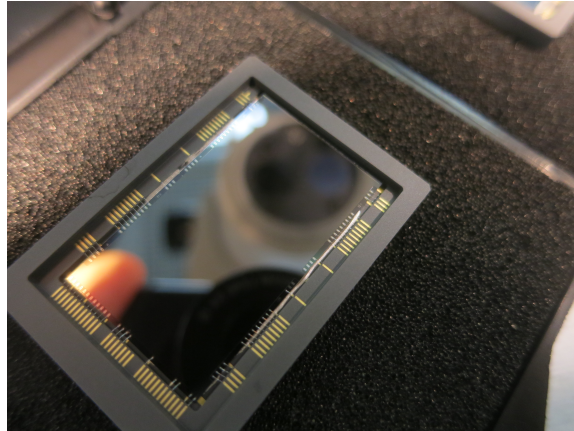
Figure 2.2: Fully packaged CCD201-20 after processing at JPL. Exposed bond pads can be seen along the edge of the silicon surface. Photo Credit Todd Jones.

gain register. Modification of the back thinning and bonding processes as well as all-wafer-level processing led to high performance with high gain and good dark current. Excellent device cosmetics were demonstrated. Quantum efficiency measurements are also underway and are expected to be further improved. A device from the most recently processed wafer is shown in Figure 2.2

2.2　JPL & Columbia Characterization & Independent Verification

Following the post-fabrication processes at JPL described above, several die (some with a single-layer AR coating) were sent to e2v for wire bonding tests and performance tests. The results from e2v showed that JPL's post-fabrication processing is compatible with e2v's packaging and wire bonding processes, with all die passing standard tests. Results also showed that the delta-doped (both bare and AR coated) devices performed as expected. The tests at e2v also independently verified QE results in the 300–700 nm range (Figure 4). E2v's setup is limited down to 300 nm. These results from e2v are an important step for the "path to flight" of delta-doped and AR-coated EMCCDs.

Sample coatings were deposited on 1 inch <100> 1–20 Ohm-cm silicon wafers (to test reflectance) and on fused silica windows (to test transmittance/absorption). For simplicity, all measurements (and corresponding models) plotted in the following figures are based on a silicon substrate without the doped layer; previous work on delta-doped CCDs has shown good fidelity to both model predictions and results from silicon wafer substrates [30, 14]. Film thicknesses were verified by spectroscopic ellipsometry (Sentech and Horiba).

Reflectance tests were conducted at Columbia University. The samples were placed in a vacuum chamber maintained at less than 1×10^{-4} Torr for the duration of the measurement. An Acton monochromator fed by a focused deuterium lamp provides illumination to the samples. The light is reflected off of silicon substrates for measuring reflectance, or directed through transparent substrates for measuring transmission. For this work, reflectance measurements were performed at 5–10° from normal. We recorded intensity using a photomultiplier tube (PMT, R6095) with a scintillator and light pipe assembly (McPherson Model 658). For each sample, the following set of measurements were made: direct intensity from the lamp, reflected intensity from the sample, reflected intensity from a bare silicon standard, reflected ambient intensity not directly in the path of the light. This last measurement is from an open filter position and serves as a background measurement. These measurements were then used to calculate direct reflectance from the sample and silicon (as a standard).

Transmission is calculated by measuring both reflectance off the silicon surface and reflectance and transmission due to the coating applied to a fused silica window. Measurements on fused silica, which also follow the model well, confirm that the behavior of the coating is as expected. To calculate absorption in the layer, we divide the measured absorption of the layer and window by the measured absorption of only the window. Any additional absorption we ascribe to the effect of the layer. This underestimates the absorption of the layer at very low wavelengths ($<$ 160 nm), where the fused silica is very absorbing. However, since our region of interest is at 195 nm and longer, we don't expect this will significantly change our results. For shorter wavelength targets, a MgF_2 window will be used. Estimated transmission is calculated by subtracting this measured absorption and previously-measured reflectance of a silicon substrate from 100%, as shown in Equation 2.1.

$$(1 - A_{\text{coating}}) = (1 - A_{\text{coating,fused Si}}) \times (1 - A_{\text{fused Si}})$$
$$T_{\text{calc}} = 1.0 - R_{\text{Si}} - A_{\text{coating}} , \tag{2.1}$$

where A_{coating} is calculated absorption due to the multi-layer coating only, $A_{\text{coating,fused Si}}$ is measured absorption due to both the coating and the fused silica window, $A_{\text{fused Si}}$ is measured absorption of an uncoated fused silica window, T_{calc} is the calculated transmission of the overall coating, and R_{Si} is the measured reflection off the coated silicon substrate.

The JPL team has developed measurement setups over the years to cover the 121.6 nm to 1,000 nm range in two systems. The far-UV system and methods of measurement are described in detail in [19]. Most of the measurements in this effort utilized the 1-m vacuum monochromator equipped with an indexable dual source (deuterium and tungsten). The half-meter monochromator system that covers the near-ultraviolet to near-infrared system was used to cross-check the results. Using these systems, QE, response uniformity, and dark current are measured routinely. Additionally, because of the stringent requirements placed on the detectors and for operating them beyond
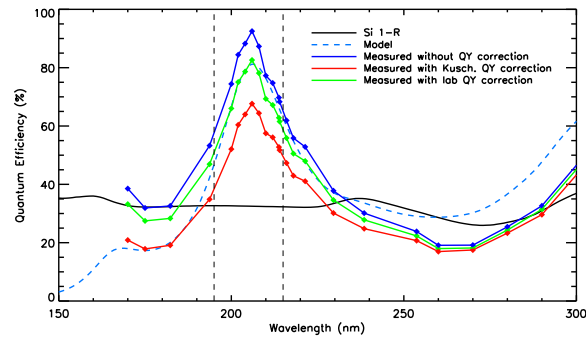
Figure 2.3: Quantum efficiency vs. wavelength for the 5-layer coating deposited on a thinned, delta-doped e2v CCD201-20. The characterization process is described in Section 2.2. Peak QE is 67.6% at 206 nm. For comparison, the uncorrected QE measurement is shown in blue. The green line shows the quantum yield (QY) corrected QE using a photon transfer method. This is likely the upper limit of QE values. We use the values derived by Kuschnerus[21] as a conservative measure of QE.

the convention, we developed additional capabilities to check more device parameters, ensuring that we could account for all photoelectrons. These efforts included establishing an additional capability to our QE setup with incorporation of an Fe-55 source for Charge Transfer Efficiency (CTE) measurements. In this KISS technology development, we have been working closely with e2v and as part of this close collaboration, device performance from two wafers were independently verified with packaging and testing at e2v. Results from QE testing at JPL are shown in Figure 2.3 [15].

2.3   Caltech Noise Performance Testing

When an EMCCD is operated in photon-counting mode, there are several additional noise sources that are not found in normal mode operation (see Section 1.3.2). The two primary sources of noise are clock induced charge (CIC) and dark current. In a standard CCD, when cooled below -85° C and with normal trapezoidal or square clocks, the noise from dark current will be only a few electrons per hour and CIC will be lower than the added read-noise (assuming a few electrons of read-noise), and thus undetectable. For an EMCCD, both of these noise sources will be amplified in the same manner as photo-electrons, and thus will be counted as events in data processing.

2.3.1   CIC

CIC is caused by impact ionization of holes as they move through the Si/SiO_2 interface during pixel clocking [1]. The amount of CIC generated depends on the clocking speed (decreasing with

increased clocking speed), the substrate voltage (more holes are in the clocks during inversion), clock overlap, and the amplitude of the clock (well depth).

In normal CCD operation, the single electrons created by clocking are normally masked by read-noise of a few electrons, and so fine tuning of the clocks is usually not necessary. In an EMCCD, electrons generated by clocking, especially in the parallel register or early in the serial register, will be amplified in the same manner as photo-electrons and can be erroneously counted as events. Thus, careful wave-shaping is required to minimize CIC. We follow Daigle [8] in reducing CIC via wave shaping and well depth adjustment. CIC in the image area is a combination of both parallel and serial CIC. CIC in over- or pre-scan regions is due only to serial CIC. Serial CIC is measured directly by counting the number of events in the over- and pre-scan regions. Parallel CIC is measured by subtracting the serial CIC value from the total number of events in the image and storage regions.

$$CIC_{\text{Parallel}} = CIC_{\text{Total, image}} - CIC_{\text{Serial, over-scan}} \qquad (2.2)$$

2.3.2 Parallel CIC

Our work to reduce CIC was conducted in several stages. First, we focused on reducing parallel CIC. Our initial waveform script used trapezoidal or square clocks, with roughly 50% overlap and well voltages from -5 to 7 V. These conditions were close to the clocking scheme specified in the e2v data sheet. Initial parallel CIC levels with this setup were 0.055 events pix^{-1} frame^{-1}, at a substrate voltage of 4.5 V. In non-inverted mode (substrate voltage of 0.0 V), the parallel CIC was much lower, dropping to 0.005 events pix^{-1} frame^{-1}.

We first experimented with reducing the clock well depths. Our initial high voltage of 7 V is the e2v recommend value. We changed both the overall well depth and the high and low voltage levels. We found that decreasing well depths to an 11 V range provided low CIC while still maintaining good charge transfer efficiency (CTE). Well depths below this voltage range caused significant degradation in the CTE. This degradation was most obvious in the central portion of the image area, which developed a hole and upward "orange peel" effect as charge was not effectively transferred through this region. Lower well depths reduced the CIC to 0.01–0.02 events pix^{-1} frame^{-1} at a substrate voltage of 4.5 V. For 0.0 V substrate, lower well depths reduced parallel CIC to 0.002 events pix^{-1} frame^{-1}.

Our second step was to shape the parallel clocks to sine instead of square clocks. This had an immediate effect on CIC, reducing it to 0.001 events pix^{-1} frame^{-1} at a substrate voltage of 4.5 V, while maintaining good CTE. This low CIC was maintained at 0.0 V substrate voltage, and due to these low values, no further wave shaping of the parallel clocks was done.

2.3.3 Serial CIC

We followed the same overall process as above to reduce the serial CIC. Initially, the serial CIC was 0.02 events pix^{-1} frame^{-1} at 4.5 V substrate, increasing to 0.05 events pix^{-1} frame^{-1} in non-inverted mode. Well depth reduction from 12 V to 10 V lowered serial CIC to 0.002 events pix^{-1} frame^{-1} at 4.5 V substrate. Finally, wave shaping lowered the serial CIC to 0.0007 events pix^{-1} frame^{-1} in inverted mode, and to 0.0005 events pix^{-1} frame^{-1} in non-inverted mode. The serial clocks used multi-step shaped clocks.

A combination of wave shaping and well depth optimization reduced total CIC to 0.0017 events pix^{-1} frame^{-1} for inverted mode and 0.0015 events pix^{-1} frame^{-1} for non-inverted mode. Table 2.1 summarizes the best results from our CIC optimization process.

		Initial Value	Reduced Well Depth	Shaped & Reduced Wells
Inverted	Parallel	0.055	0.02	0.001
	Serial	0.02	0.002	0.0007
	Total	0.075	0.022	0.0017
Non-Inverted	Parallel	0.005	0.002	0.001
	Serial	0.05	0.005	0.0005
	Total	0.055	0.007	0.0015

Table 2.1: Table summarizing CIC measurements for inverted (4.5 V substrate voltage) and non-inverted (0.0 V substrate voltage) operating modes, both before, during, and after optimization.

2.3.4 Dark Current

Dark current can be reduced by operating in inverted mode and by cooling the device. Recent work exploring dark current vs temperature indicate a lower limit to dark current [33, 6], however most applications operate at -85° C and the behavior below this temperature has not been extensively investigated. Additionally, cold operation of the CCD leads to a significant reduction in charge transfer efficiency (CTE). Keeping these limits in mind, we explore dark current in both an engineering grade and delta-doped EMCCD.

Our work investigated dark current at CCD temperatures between -85 and -125°C. Our setup has a temperature sensor at the back of the CCD copper clamp, which was typically 3°C below the CCD temperature. Thus, a clamp temperature of -88°C corresponds to a CCD temperature of -85°C. We found a difference in dark current between the image area and the storage area of the frame transfer e2v CCD201-20. The exact reason for this difference is not clear, but may be related to the differing thickness of the areas or to passivation of the back surface by the
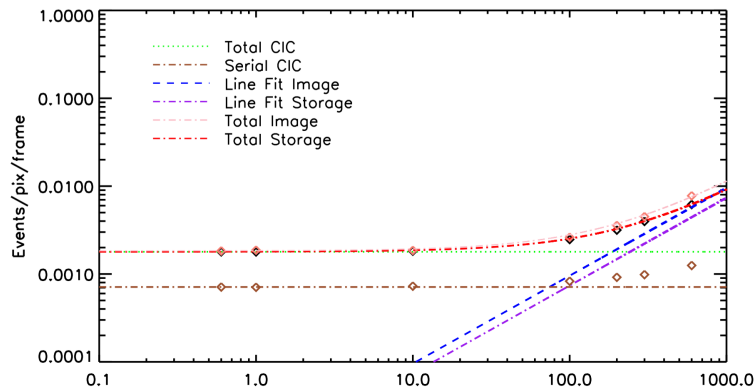
Figure 2.4: Typical dark current measurement. This example is taken at -108°C. The green and brown lines indicate total and serial CIC, respectively. The blue and purple lines indicate a least-squares line fit to the CIC subtracted data. Finally, the pink and red lines indicate the total fit with both CIC and dark current for the image and storage areas of the device. Data points are shown as diamonds. Temperatures refer to the CCD clamp back and thus are 3°C cooler than the CCD surface.

aluminum storage shield. We found that the storage area had a dark current roughly half that of the image area.

We measured dark current after optimizing for low CIC as described in Section 2.3.1. Dark current tests were conducted after a standard turn-on procedure designed to minimize so-called "injected charge," which appeared in the device as elevated dark current after the controller was reset [33]. The device was turned on at room temperature and allowed to read out for 24 hours, at which point the device was cooled, while being continuously read out, to -85°C for the first dark current test. Turning the controller off and on while the device was cold caused dark current to increase and then slowly decay at a rate that varied with temperature. To avoid this effect, we did not power cycle the controller during dark measurements.

Dark current was measured by taking a set of exposures at increasing exposure times, with five to ten images per exposure time. The high voltage gain was set to 1,000 e/e, or as close to this value as possible. The number of events per frame was extracted using a 5σthreshold and averaged for exposure time. Over-scan and pre-scan regions were also read out for each image. The number of events due to CIC for each set was extracted from the zero second exposure. Additional events with increasing exposure time are attributed to dark current, after cosmic ray removal. For each temperature and substrate voltage configuration, CIC events were subtracted from the total number of events. Then a dark current rate was measured using a least-squares line fit to the remaining counts. The dark current was calculated for both the image and storage area. An example of this measurement is shown in Figure 2.4.
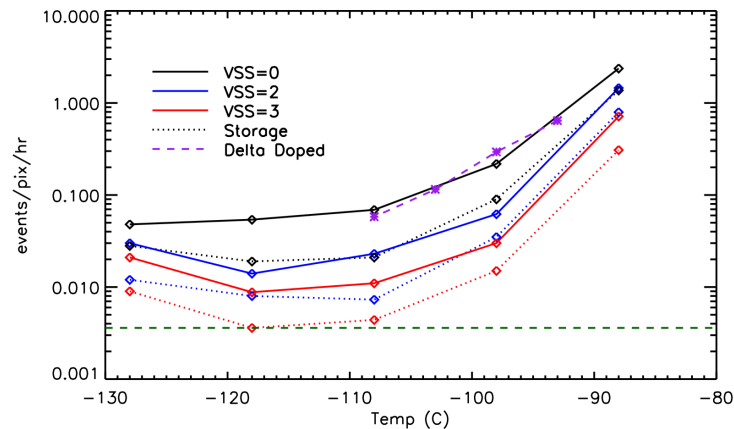
Figure 2.5: Measured values of dark current vs. temperature. Solid lines indicate dark current for the image area, while dotted lines indicate dark current for the storage area. Colors represent different substrate voltages. Initial dark current measurements of a delta-doped device are shown in purple at a substrate voltage of 0.0 V.

The dark current measurements we show here are preliminary. These images were processed using a de-smearing technique to eliminate smeared pixels and reconstruct the un-smeared events. Furthermore, at colder temperatures, cosmic rays become increasingly large sources of noise. The decreased CTE causes cosmic ray events to be smeared out over many pixels. For dark current measurements, these pixels are excised by hand and the rates are corrected to account for the lost pixel numbers.

For the engineering-grade e2v CCD201-20, we found that dark current decreased with temperature until -105°C. At -85°C, our results agree well with those from Tulloch[33] and Daigle[6]. Below this, there appeared to be a plateau where lower temperature did not significantly reduce dark current. Both image and storage areas exhibited this plateau. Variations in the voltage substrate reduced dark current, as the device is lowered into inversion. Increasing the substrate voltage decreased dark current, while still maintaining the plateau, although the exact value of the plateau did decrease. The plateau may be due to a combination of a low level light leak plus a non-temperature-dependent component that varies with substrate voltage. Further tests are required to determine the factors contributing to the plateau.

Dark current test results are summarized in Figure 2.5.

Initial testing of the performance of a delta-doped device is still ongoing and is not as far along as the engineering-grade device testing. Thus, we restrict our results to initial dark current measurements at a single voltage substrate (0.0 V). We find that the delta-doped device dark current performance is comparable to that of the engineering-grade device dark current. These devices do not have a storage shield and operate in full frame (1k × 2k). Dark current
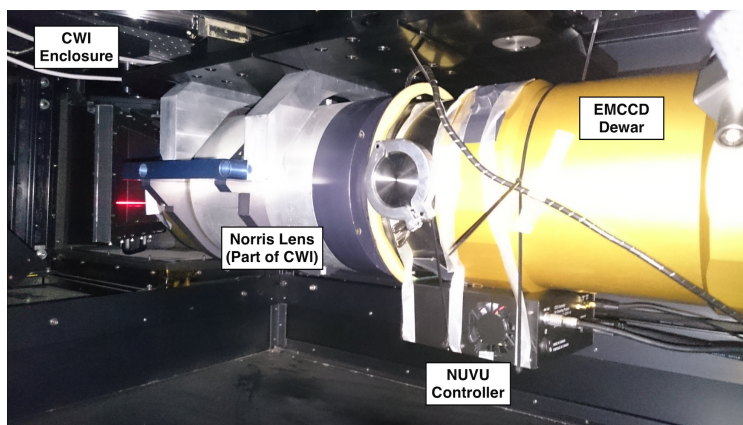
Figure 2.6: Picture inside CWI enclosure of the EMCCD dewar attached to the Norris Lens of CWI. The NUVU controller can be seen at the bottom of the dewar.

measurements are from the whole device region. Measurements are plotted on Figure 2.5 as the dashed purple line and purple x's.

2.4   On-Sky Tests

2016 will be a banner year for tests of high efficiency UV EMCCDs. We will conduct two different on-sky tests: one at visible wavelengths with a slicer integral field unit at Palomar, the Palomar Cosmic Web Imager (PCWI), and another at UV wavelengths with the flight of FIREBall-2 in the fall of 2016. FIREBall-2 is a multi-object spectrograph observing between 200 and 210 nm. Testing the devices on FIREBall-2 is a clear next step for flight qualification and future use on UV/VIS space telescopes. Testing the devices on PCWI is a good way to evaluate observing modes and can also serve as initial tests with an eye toward one day replacing the PCWI detector with a blue optimized EMCCD.

2.4.1   First Tests of EMCCD Devices at Palomar

An EMCCD operating with PCWI would eliminate the need for both masking and for CCD shuffling. Instead, fast cadence observations of the object and sky would be read out as they are completed, every two minutes or so, with little read noise added. The entire CCD can be used with no loss of S/N, increasing the efficiency of PCWI in nod-and-shuffle mode by a factor of three. Furthermore, this means that H-β and the OIII doublet, or H-α and the SII doublet, can be observed simultaneously, without compromising sky subtraction; PCWI is currently not capable of this with its existing detector. In general, a data sequence using nod-and-shuffle mode takes about 50 minutes, and there are a number of ways in which the data can be compromised.

Poor seeing, cloud cover during the acquisition, or telescope operation/guiding lost can all ruin a sequence, wasting an hour of observation.

EMCCDs are capable of almost eliminating read noise, meaning that relatively short exposures can be used and read out while nodding the telescope. This capability would allow the observer to terminate the sequence at any point without loss of data. A shorter readout cadence also means the evolution of the sky can be tracked every few minutes. The PCWI data reduction pipeline could perform a more dynamic fit, with improved sky subtraction. Non-linearity in the sky signal could be determined over an observing period. Shorter time between readouts would also reduce the impact of flexure within a single exposure. During longer integrations, PCWI experiences a 10% degradation in spectral resolution in the form of flexure-smeared lines. This effect can be greatly reduced using an EMCCD with a short exposure time and readout.

The observing run with PCWI went very well, especially given the time frame within which we were working. The dewar behind CWI is shown in Figure 2.6. Some modifications were made to the mechanical components to ensure that the FIREBall dewar and detector matched with the current setup. Unfortunately, our laboratory dewar did not match in size to that used for the PCWI detector. The overall length was increased, and thus our grating and detector angles were limited. As this test was an engineering and calibration run, this discrepancy did not impact our scientific justification. The device performed excellently and our installation was very smooth. There were no adjustments required once installed. The detector-to-instrument focus was almost perfect; any offsets were minor and were corrected internally, as would happen with a grating switch using the normal detector.

This run was an important test of how a delta-doped device performs on sky. It was also hugely important for us to test our communications system and software, both using the detector at a terminal level (not using the built-in GUI) and finding out what worked best with the opto-mechanical system currently in use. During the day, we made improvements to our data acquisition software from findings over the night. We have also, since this run, developed a server-based environment, which allows us to reduce our overheads during acquisition.

Our preparation for upcoming runs of this kind (May 2016) will be further streamlined in software, but our main changes are in hardware and the use of a device that will better match that of a qualified flight device. The device used in November 2015 was the first available JPL, delta-doped device with minimal cosmetics; however, it was not deemed an ideal candidate for our balloon flight, based on engineering testing at JPL and our own laboratory testing. Current testing of newly processed devices are underway, one of which will be used on the next observing run.

2.4.2 Integration of Devices into FIREBall-2

The second on-sky test will occur next summer. The FIREBall-2 balloon project [36, 26] will be the first flight of a UV-optimized, delta-doped EMCCD in a flight setting. The spectrograph is currently being integrated in Marseille, and is designed to observe at the 200–210 nm balloon window. FIREBall-2 will target the bright CGM around $z \sim 0.7$ galaxies and will take the first UV spectra with a multi-object spectrograph. This flight will serve as a testbed for future UV space missions. We hope to fly FIREBall-2 several more times after the summer 2016 flight, and will be able to conduct additional flight tests of UV-optimized delta-doped EMCCD detectors. Optimizing observing modes and cadences, determining the best way to take calibrations, testing detector configurations, and UV-coatings will all be key components that will be tested during and between flights.

2.5 Papers, Published Work, & Presentations

Two book chapters:

1. "High-performance silicon imagers and their applications in astrophysics, medicine and other fields," Shouleh Nikzad, in *High Performance Silicon Imaging: Fundamentals and Applications of CMOS and CCD Image Sensors*, D.Durini, ed. (Elsevier), pp. 411–438.

2. "Digital Imaging for Planetary Missions," Shouleh Nikzad, April Jewell, Alex Carver, Michael Hoenk, L. Doug Bell, and Justin Maki, in the *Handbook of Digital Imaging*, edited by M. Kriss. John Wiley & Sons, Ltd: Chichester, UK, pp. 1531–1558.

Three SPIE papers:

1. "High efficiency CCD detectors at UV wavelengths," Erika T. Hamden, April D. Jewell, Samuel Gordon, John Hennessy, Michael E. Hoenk, Shouleh Nikzad, David Schiminovich, D. Christopher Martin, *SPIE* 9144 (June 2014).

2. "Detector Preformance for the FIREBall-2 UV experiement," April D. Jewell, Erika T. Hamden, Hwei Ru Ong, John Hennessy, Timothy Goodsall, Charles Shapiro, Samuel Cheng, Todd Jones, Alexander Carver, Michael Hoenk, David Schiminovich, Christopher Martin, Shouleh Nikzad. *SPIE* 9601 (August 2015)

3. "Noise and dark performance for FIREBall-2 EMCCD delta-doped CCD detector," Erika T. Hamden, Nicole Lingner, Gillian Kyne, Patrick Morrissey, D.Christopher Martin, *SPIE* 9601 (August 2015)

One referred paper submitted:

1. "CCD Detectors with high Quantum Efficiency at Ultraviolet Wavelengths," Erika T. Hamden, April Jewell, Tim M. Goodsall, John Hennessey, Shouleh Nikzad, Michael Hoenk, Todd Jones, Sam Gordon, David Schiminovich, D. Christopher Martin, in preparation for submission to *JATIS*, April 2015

Presentations

1. "Detectors and Advanced Coatings for Efficient UV/Optical/NIR Systems," S. Nikzad, M.E. Hoenk, A. Carver, T.J. Jones, J. Hennessy, A. Jewell, E. Hamden, & T. Goodsall, *Scientific Detector Workshop*, Florence, Italy October 7-9 2013.

2. "High-Performance Silicon Imaging Arrays for Cosmology, Planetary Sciences, and other Applications," Shouleh Nikzad, et al. (2014), Invited Talk and Paper in *International Electron Devices Meeting*.

3. "From Nebulae to Neurons: Using Nanoengineering to Produce High Performance Imaging Arrays for NASA Missions, Machine Vision, and Medical Applications," Shouleh Nikzad, Colloquium Presentation, School of Earth and Space Exploration, Arizona State University, Tempe, AZ, 12 February 2014.

4. "High Efficiency Detector Arrays and High Reflectivity Optical Coatings for High Performance Ultraviolet and Optical Instruments," Shouleh Nikzad, Astronomy Department Technical Talk, Arizona State University, Tempe, AZ, 13 February 2014.

5. Two posters at *SPIE Astronomical Telescopes and Instrumentation* (Montreal, June 2014)

6. One oral presentation at *SPIE Astronomical Telescopes and Instrumentation* (Montreal, June 2014)

7. Three oral presentations at *SPIE Optics + Photonics* (San Diego, August 2015)

8. Three presentaions at *SPIE Astronomical Telescopes and Instrumentation* (Edinburgh, June 2016)

2.6   External Funding Proposed & Received

The original KISS Study and the subsequent technology development fund has been excellent for forging collaborations and starting new areas of research. Some of the examples are listed below:

1. "High Efficiency Detectors for Photon Counting & Large FPAs", ROSES-SAT.

2. "Advanced Coatings Enabling High Performance Instruments for Astrophysics Missions," NASA ROSES-Astronomy and Physics Research and Analysis, 2015-2017, PI Shouleh Nikzad.

3. "Advanced FUV/UV/Visible Photon Counting and Ultralow Noise Detectors," Shouleh Nikzad, Michael E. Hoenk, Chris Martin, and David Schiminovich, Strategic Astrophysics Technology (SAT)— 2016-2018.

4. "Advanced Ultraviolet Spectrometer," Primitive Bodies Strategic Initiative Research & Technology Development (RTD) – 2012-2014.

5. "Compact Ultraviolet Imaging Spectrometer for Planetary Systems", Shouleh Nikzad, Alex Carver, Pantaziz Mouroulis, Dan Wilson, Robert West, Walter Harris, Strategic Initiative Research and Technology Development (RTD) – 2016-2018.

6. "FIREBall-2: Pioneering Space UV Baryon Mapping," ROSES-APRA PI Christopher Martin, 2015-2017

7. "EMCCD technology for ultraviolet astronomy and high resultion spectroscopy," RTF, PI Erika Hamden, 2015

SAT = Strategic Advanced Technology
APRA = Astronomy and Physics Research and Analysis
RTD = Research and Technology Development

Our KISS Study that spawned this technology development also created several other activities. These include start of new collaborations and funded research projects based on the recommended technical areas highlighted in the study report. This includes study participant Paul Scowen, who was invited to be on the COPAG. He has subsequently been leading the COPAG-SIG#2 which will provide material for the upcoming decadal survey report.

Shouleh Nikzad and Kevin France started a new collaboration (they met for the first time at the workshops) and now have a funded APRA to develop optical reflective mirror coatings in the ultraviolet. Paul Scowen and Matt Beasley have begun an ALD-based work funded by NASA-SAT.

Doug Bell and Shouleh Nikzad led a Center Innovation Funds (CIF)-supported workshop and study on Metamaterials for UV instruments. Participants included David Schiminovich, Kevin France (both from the KISS STUDY) and Walt Harris (U of Arizona) and Nader Engheta (U of Penn). This has resulted in small seed funding for further calculations and small fabrication areas.

CHESS a sounding rocket at Colorado was funded (Kevin France) and will fly a delta-doped detector, although optimized at a different wavelength range than the detectors described here.

Finally, postdoctoral fellow Erika Hamden was recently awarded a Nancy Grace Roman Technology Fellowship (RTF) for a proposal to provide flight qualification of the UV-optimized CCDs. The RTF provides funding for lab equipment and will also be used to hire additional graduate students.
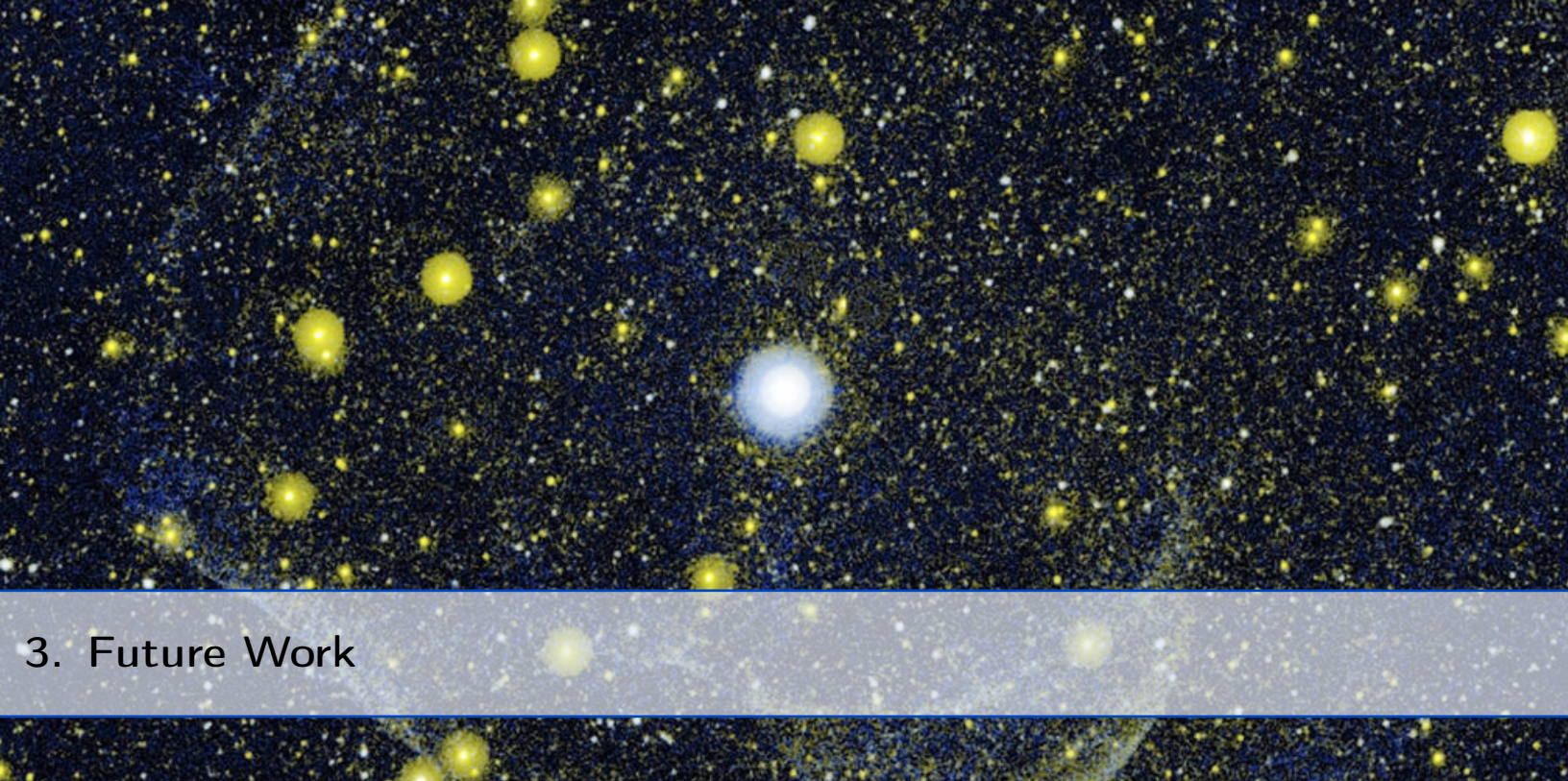
3. Future Work

High efficiency EMCCD detectors have great potential to increase instrument throughput, lower costs, and increase sensitivity at UV/VIS/near-IR wavelengths, and can make an immediate, large impact when used at UV wavelengths in particular. The Association of Universities for Research in Astronomy (AURA) recently released a report on a future large scale UV/VIS space telescope [9]. When identifying essential UV technologies of the future, especially in light of the eventual end of the Hubble Space Telescope (HST) mission, they describe the need for a detector that can achieve the "triple crown...high quantum efficiency, low read noise/photon counting, and low dark current." High efficiency, UV-optimized EMCCD detectors will meet these challenges.

3.1 Upcoming & Long-Term Proposal Opportunities

Since the 2010 Decadal Survey was released, there have been several updates and mid-decadal reports on the state and outlook of astronomy, especially as it connects to the goals outlined in New Worlds New Horizons (NWNH, National Research Council 29). These reports highlight important science drivers and technology priorities in anticipation of the 2020 Decadal Survey. Two reports were recently released by the Association of Universities for Research in Astronomy (AURA) and the Cosmic Origins Program Analysis Group (COPAG) to provide guidance on future technology development. The AURA report [9] in particular focused on a future 12-m class space telescope operating at both UV and visible wavelengths with multiple instruments. The stated goal, "to find and characterize dozens of Earth-like planets and make transformational advances in astrophysics," is the primary driver of the recommended technologies in the report. The COPAG Annual Technology Review (ATR, `http://cor.gsfc.nasa.gov/docs/2015CORPATRRev1.pdf`) continues to be informed by the suggestions of NWNH, including the recommended Habitable

Exoplanet Imaging Mission. In both cases, the additional science targets beyond exo-earth discovery are understanding galaxy evolution, the evolution of star formation, stellar evolution, and discoveries within our own galaxy and solar system.

One technology gap called out in particular and highlighted by both reports is the need for high QE, radiation-hard, large-format UV and visible detectors for both photon counting and normal mode operation (Table 3.1 in COPAG report). UV-optimized EMCCDs will fill this technology gap. The emphasis on increasing the technology readiness levels (TRL) of these detectors quickly, both before the next Medium-class Explorer (MIDEX) call in 2016 and before the 2020 Decadal Survey (Priority 1.4-6), is a priority that this funding has directly supported and is a significant reason why these detectors are gaining a higher profile.

3.1.1 MIDEX AO in winter 2016

At the end of 2016, our group will propose a Medium-class Explorer (MIDEX) designed to detect and study emission from the nearby CGM and IGM. This mission, ISTOS, hinges in large part on the performance of these detectors, since the detection of this faint material is predicated on the high QE and low noise that EMCCDs can achieve. The KISS funded work to develop and test the EMCCDs has eliminated many major and minor weaknesses related to detector reliability and performance in advance of the future MIDEX AO.

3.1.2 Future Large-Scale UV/VIS Telescope

The AURA [9] report calls for a baseline detector that is essentially a high-performance UV-optimized EMCCD: high QE, low noise, photon counting, and UV sensitivity. This report was written with an eye toward influencing Decadal Survey priorities, especially in technology development. Ensuring future UV access is also a priority for AURA, especially in light of the eventual end of COS/HST. Table 5-1 in the report shows the importance of UV capability for nearly all science drivers and epochs, including detecting star formation in galaxies, detecting emission from gas accreting and being blown out of galaxies, determining the UV mass function of young clusters, understanding protostellar disk abundances and accretion, and detecting emission from exoplanets. Later in the report, there is a discussion of the UV detector required to achieve all of these science targets (Section 5.2.3). As described earlier, UV-optimized EMCCDs can achieve the detector "triple crown" recommended by the AURA report. Development of high QE, low noise, photon counting UV detectors is of the highest priority (Table 6-2) and a strong investment now in their development is highly recommended. Similarly, the ATR report recommends technology funding to increase TRL of "Photon-Counting Large-Format UV Detectors" and "High-QE, Rad-Hard, Large-Format, Non-Photon-Counting UVOIR Detectors," both niches where UV-optimized EMCCDs can fill technology gaps. Both reports provide strong support for a technology program to increase TRL for UV-optimized EMCCDs.

3.1.3 2020 Decadal Survey

At the winter American Astronomical Society (AAS) meeting in Kissimee Florida, NASA announced the formation of large mission concept study teams in anticipation of the 2020 Decadal Survey. These teams would focus on a Far IR Surveyor, a Habitable-Expolanet Imaging Mission, a Large UV/Optical/IR Surveyor, and an X-ray Surveyor. NASA anticipates that the Decadal Survey committee will use the work of these four studies to formulate recommendations for the next large-scale NASA mission beyond WFIRST and JWST. Several members of the KISS Study have applied to work on the UVOIR and exoplanet surveyors, since these benefit the most from the incorporation of UV optimzed EMCCDs.

3.2 Expected Future Technology Development

The next several years should bring UV-optimized EMCCDs to the forefront of UV astronomy. If selected as part of a MIDEX mission, these detectors will be thoroughly tested beyond the procedures outlined here. In addition, upcoming tests will provide further verification of device performance.

3.2.1 EMCCD Sky Tests Using CWI on Palomar

Additional on-sky tests will be conducted in 2016 using CWI at Palomar. Four nights are scheduled for May 2016, with a proposal in for 2016B nights. With fit checks and general engineering requirements satisfied in the 2015 observing run, these nights will focus on observing modes. We will continue modification of the nod and shuffle observing sequence as needed, determine ideal exposure times given sky background levels, test an upgraded low-noise PCB, and make photon-counting observations for blue targets. We will also be able to independently measure the QE of the detector by comparing standard stars observations.

### 3.2.2 FIREBall-2 Flight in 2016

The early fall 2016 flight of FIREBall-2 will provide the first on-sky test in the UV. This is a crucial test in determining overall performance and verifying such quantities as: sky background levels, bright CGM emission levels, fill factor for CGM emission, and fraction of observed galaxies with CGM emission. We will also test other technology components, including the NUVU controller, Sunpower Cryotel cryocooler, and updated grating.

3.2.3 Roman Fellowship Detector Testing Lab

The Roman Fellowship Detector testing lab, set up by postdoctoral fellow Erika Hamden, will provide for additional testing of the detectors. This testing includes an independent QE characterization system using a UV integrating sphere, further dark current testing in an ultra-dark vacuum setup, low-noise PCB design and testing, along with testing of the NUVU v3 controller with slower clocking speeds.

3.2.4 Future APRA/SAT Funding

The PIs and collaborators plan to conduct additional flights of the FIREBall-2 balloon after 2016, with an upcoming APRA proposal requesting funds for a flight in 2018. The potential for a spring flight from the southern hemisphere would yield additional targets of great interest for CGM science. An additional APRA proposal for multiple AR coatings per detector will also be submitted.
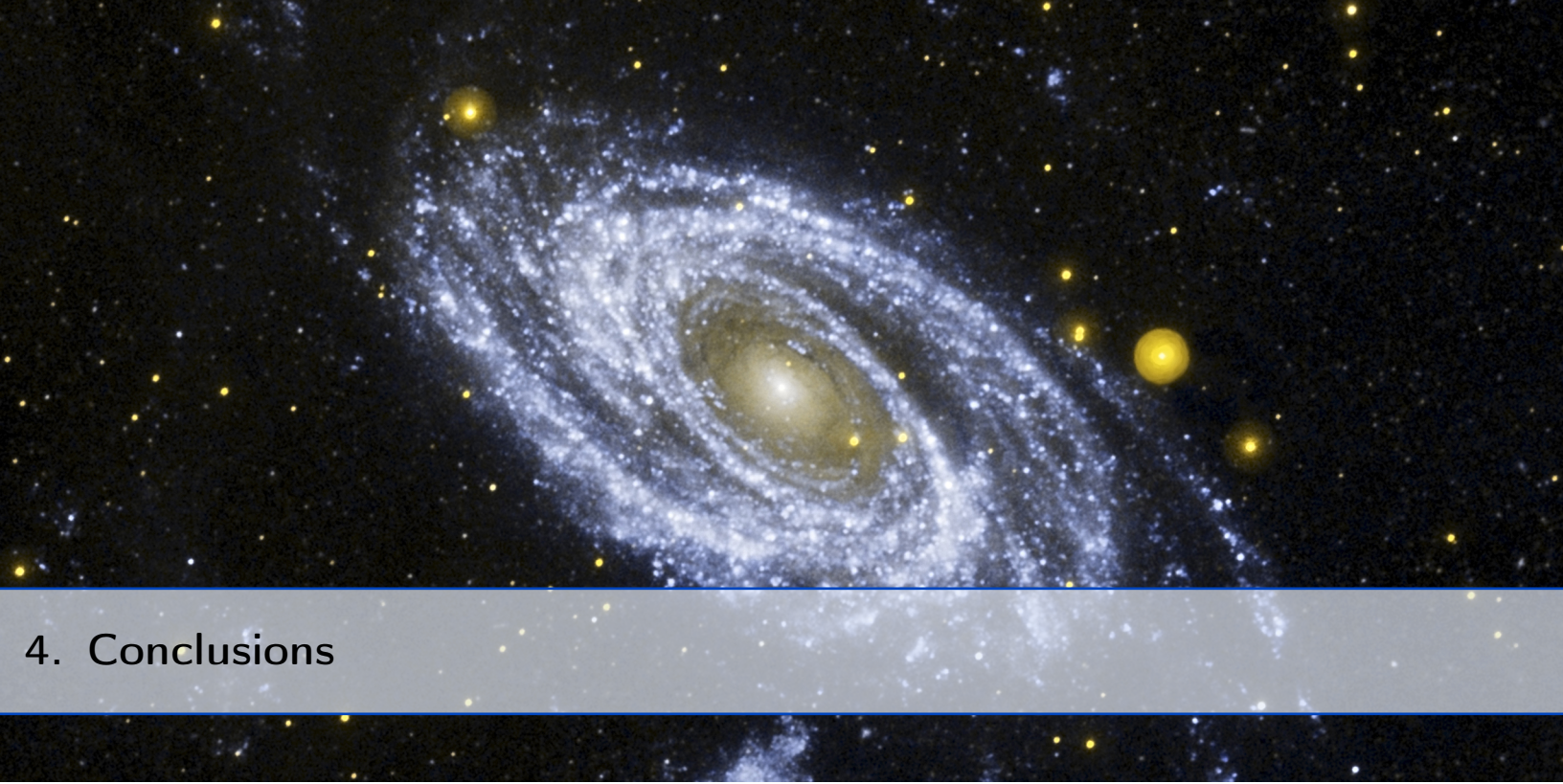
4. Conclusions

This development work has yielded exciting scientific results and has led to the development of high-efficiency, low-noise photon counting UV CCD detectors, including several potential flight detectors. This success is due to the efforts of all members of the collaboration, with extensive testing conducted at JPL, Caltech, and Columbia University. Based on the results of this development, we expect flight tests of UV-optimized EMCCDs to start in 2016, with more in the future.

We successfully delta-doped several wafers of large area array e2v EMCCD CCD201-20s, applying multi-layer ARCs to increase QE above 70%, with independent QE verification. We demonstrated end-to-end wafer-level EMCCD processing. We have extensively tested the noise properties of an engineering-grade device and are finalizing noise testing of UV-optimized EMCCDs. On-sky testing at Palomar with CWI has already started and future on-sky tests are planned for 2016, including the flight of a UV balloon telescope.

This detector (or ones very much like it) will be proposed for use on a future MIDEX mission and are likely to form the baseline detectors for larger missions in the medium- to far-term.
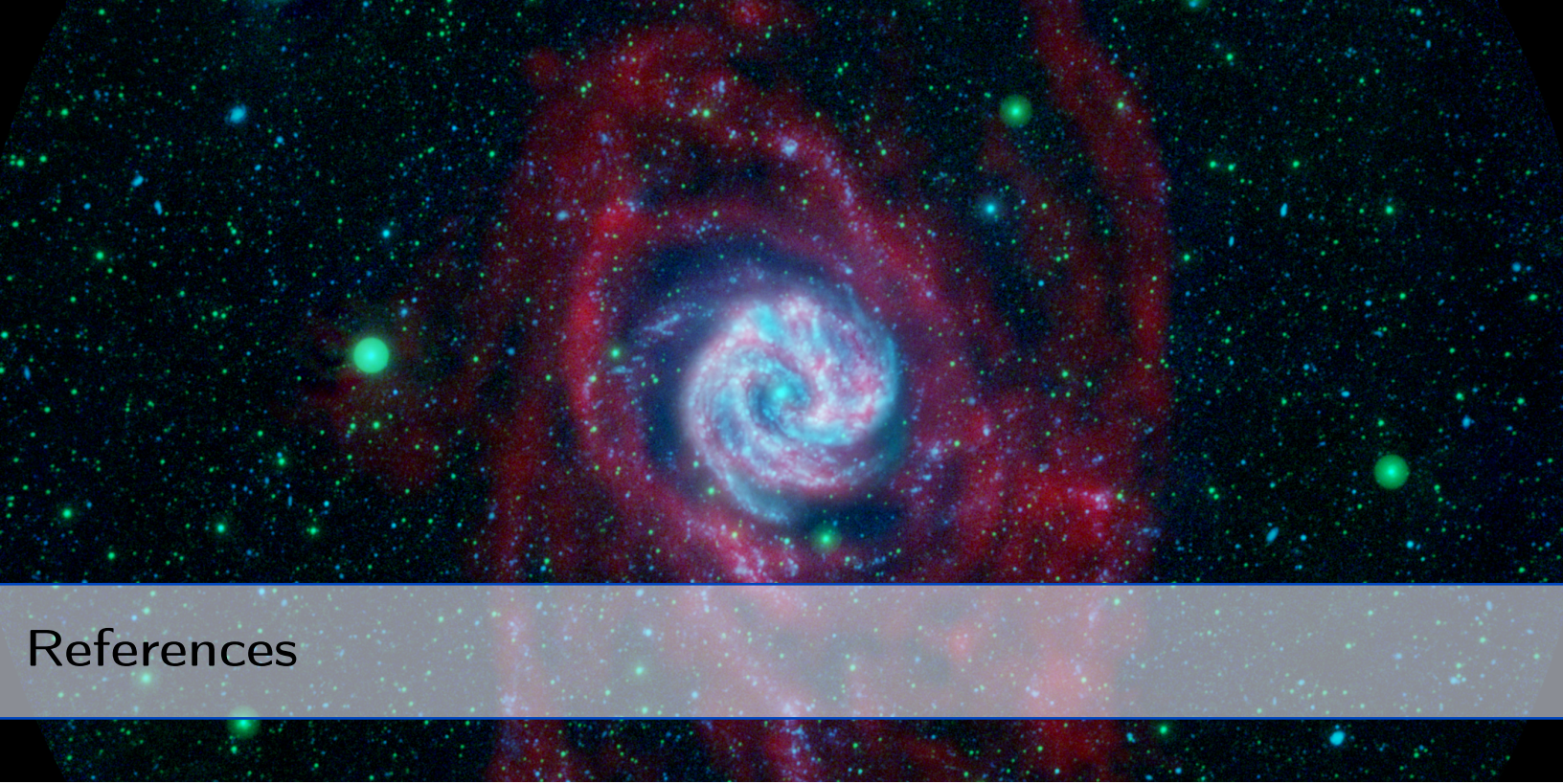
References

[1] 2015, Low-Light Technical Note 4, Tech. Rep. A1A-Low-Light_TN4 Version 3, e2v Technologies, Chelmsford, UK

[2] Bonfond, B., et al. 2015, Ann.Geo., 33, 1211

[3] Borucki, W. J., et al. 2011, The Astrophysical Journal, 736, 19

[4] Bouwens, R. J., et al. 2011, Nature, 469, 504

[5] Cantalupo, S., et al. 2014, Nature, 506, 63

[6] Daigle, O., et al. 2012, Vol. 8453 of SPIE

[7] Daigle, O., et al. 2008, Vol. 7014 of SPIE

[8] Daigle, O., et al. 2010, Vol. 7742 of SPIE

[9] Dalcanton, J., et al. 2015, arXiv:1507.04779

[10] Day, P. K., et al. 2003, Nature, 425, 817

[11] Ford, A. B., et al. 2015, ArXiv e-prints, arXiv:1503.02084

[12] Gladstone, G. R., et al. 2014, Space Science Reviews, doi:10.1007/s11214-014-0040-z

[13] Green, J. C., et al. 2012, ApJ, 744, 60

[14] Hamden, E. T., et al. 2011, Applied Optics, 50, 4180

[15] —. 2016, submitted to JATIS

[16] Harpsøe, K. B. W., et al. 2012, A&A, 537, A50

[17] Hennawi, J. F., et al. 2006, ApJ, 651, 61

[18] Hummels, C. B., et al. 2013, MNRAS, 430, 1548

[19] Jacquot, B. C., et al. 2010

[20] Kang, Y., et al. 2012, ApJS, 199, 37

[21] Kuschnerus, P., et al. 1998, Metrologia, 35, 355

[22] Martin, C., et al. 2003, Vol. 4854 of Presented at the SPIE Conference

[23] Martin, D. C., et al. 2014, ApJ, 786, 106

[24] —. 2015, Nature, 524, 192

[25] Mazin, B. A., et al. 2013, PASP, 125, 1348

[26] Milliard, B., et al. 2010, Vol. 7732 of SPIE

[27] Moos, H. W., et al. 2000, The Astrophysical Journal Letters, 538, L1

[28] Morrissey, P., et al. 2005, The Astrophysical Journal Letters, 619, L7

[29] National Research Council. 2010, New Worlds, New Horizons in Astronomy and Astrophysics (Washington, DC: The National Academies Press)

[30] Nikzad, S., et al. 2012, Appl. Opt., 51, 365

[31] Rudie, G. C., et al. 2012, ApJ, 750, 67

[32] Siegmund, O. H. W., et al. 2011, Advances in microchannel plates and photocathodes for ultraviolet photon counting detectors, doi:10.1117/12.894374

[33] Tulloch, S. 2010, PhD thesis, The University of Sheffield

[34] Tulloch, S. M., & Dhillon, V. S. 2011, MNRAS, 411, 211

[35] Tumlinson, J., et al. 2013, ArXiv e-prints, arXiv:1309.6317

[36] Tuttle, S. E., et al. 2008, Vol. 7014 of Presented at the SPIE Conference

[37] Werk, J. K., et al. 2014, ApJ, 792, 8